https://doi.org/10.1016/j.jaerosci.2022.105995

Infection control measures for public transportation derived from the flow dynamics of obstructed cough jet

*C. T. Wang[1,2], J. C. Xu[2], K. C. Chan[1], H. H. Lee[3], C.Y. Tso[3], Carol S. K. Lin[3], Christopher Y. H. Chao[1,4], S. C. Fu[1]**

[1] *Department of Mechanical Engineering, The University of Hong Kong, Hong Kong, China*

[2] *Department of Mechanical and Aerospace Engineering, The Hong Kong University of Science and Technology, Hong Kong, China*

[3] *Department of Energy and Environment, City University of Hong Kong, Hong Kong, China*

[4] *Department of Building Environment and Energy Engineering & Department of Mechanical Engineering, The Hong Kong Polytechnic University, Hong Kong, China*

Corresponding email: scfu@hku.hk

ABSTRACT

During the COVID-19 pandemic, WHO and CDC suggest people stay 1 m and 1.8 m away from others, respectively. Keeping social distance can avoid close contact and mitigate infection spread. Many researchers suspect that suggested distances are not enough because aerosols can spread up to 7-8 m away. Despite the debate on social distance, these social distances rely on unobstructed respiratory activities such as coughing and sneezing. Differently, in this work, we focused on the most common but less studied aerosol spread from an obstructed cough. The flow dynamics of a cough jet blocked by the backrest and gasper jet in a cabin environment was characterized by the particle image velocimetry (PIV) technique. It was proved that the backrest and the gasper jet can prevent the front passenger from droplet spray in public transportation where maintaining social distance was difficult. A model was

developed to describe the cough jet trajectory due to the gasper jet, which matched well with PIV results. It was found that buoyancy and inside droplets almost do not affect the short-range cough jet trajectory. Infection control measures were suggested for public transportation, including using backrest/gasper jet, installing localized exhaust, and surface cleaning of the backrest.

Keywords: COVID-19; Gasper jet; Jet interaction; Particle image velocimetry; Public transport

Abbreviations

B_1, B_2,.. B_9,	Position on back surface of backrest	d	Diameter of cough jet
HP	Healthy passenger	d_0	Initial diameter of cough jet
IMI	Interferometric Mie imaging	dt	Discrete time
IP	Infected passenger	h	A constant
MERS	Middle east respiratory syndrome	k	A constant
PIV	Particle image velocimetry	m_{cj}	Mass of cough jet
PVC	Polyvinyl Chloride	m_{gj}	Mass of gasper jet
SARS	Severe acute respiratory syndrome	ρ	Density of air
T_1, T_2, T_3	Position on top surface of backrest	ρ_{cj}	Density of cough jet
V	Vertical velocity of cough jet	ρ_{gj}	Density of gasper jet
V_{cj}	Horizontal velocity of cough jet	x	Coordinate in x direction
V_{gj_max}	Vertical centerline velocity of gasper jet	x_0	x position of gasper jet
V_{gj}	Vertical velocity of gasper jet	y	Coordinate in y direction

1. Introduction

Due to the outbreaks of the severe acute respiratory syndrome (SARS), middle east respiratory syndrome (MERS), and COVID-19, respiratory disease transmission and control have attracted

increasing interest [1-3]. Respiratory activities of an infected passenger such as coughing are the sources of respiratory viruses or bacteria. The expiratory droplets together with the air from the lung were released from people's mouths forming a strong cough jet. The jet of coughing or sneezing has high momentum and contains numerous aerosols [4,5]. Thus, the virus-laden large droplets can spread up to around 2 m away from the infected person before deposition on the ground [6-9]. Thus, during the COVID-19 pandemic, WHO and CDC suggest people stay 1 m and 1.8 m (i.e. 6 feet) away from others respectively to avoid the droplet route during close contact [10,11]. At the same time, many researchers suspect that the suggested social distances are not enough to mitigate infection spread because the aerosols can travel up to 7 m - 8 m away from the infected person [12,13] and aerosol transmission is an important route for the COVID-19 [14-17]. Overall, these suggested social distances are based on droplet or aerosol spread from the unobstructed coughing or sneezing jet in a large space. However, in some situations, the cough jet can be blocked and change travel direction, and the aerosols may not be transported far away as expected. For example, in public transportation, the cough jet may impinge on the front backrest or be affected by the overhead gasper jet. This is a different scenario from the unobstructed coughing or sneezing jet. Thus, studies of the flow dynamics of cough jets in public transport cabins can help to understand the special aerosol dispersion and develop infection control measures in public transportations.

So far, many researchers have characterized or visualized the unobstructed cough jet from different perspectives such as velocity field [5,18-21], droplet evaporation and dispersion [6,22-24], and penetration distance [6,13,25,26]. Some researchers characterized the flow dynamics of human cough immediately near the mouth. Chao et al. [5] studied the initial velocities and size distributions of cough droplets from male and female volunteers by particle image velocimetry (PIV) and interferometric Mie imaging (IMI). Gupta et al. [19] studied the flow rate, jet direction, and mouth opening area of the human cough. Tang et al. [21] visualized the

unobstructed initial cough airflow near the volunteer by the schlieren imaging technique and studied the effect of masks on the cough jet. Some researchers used an analytical approach to model the cough droplet evaporation and dispersion. Xie et al. [6] modeled the evaporation and dispersion of a single cough droplet and studied the traveling distance of cough droplets under different humidity and droplet size. Redrow et al. [24] modeled the evaporation and dispersion of airborne cough droplets by considering the chemical components and the probability density function. Wei and Li [23] modeled the spread of expiratory droplets from a cough by considering the turbulence. Liu and Novoselac [27] studied the transport of airborne particles from a cough jet and evaluated the penetration distance and velocity of the cough jet. Some researchers used experimental methods to study the flow field of a cough jet. Vansiver et al. [18] characterized the human cough flow field using PIV, including the releasing velocity, velocity profile with distance, and cough width. Bourouiba et al. [25] captured droplet movement from human cough and sneeze by a camera and theoretically analyzed the droplet movement in the cough cloud by discrete and continuous models. Dudalski et al. [20] investigated the far-field human cough airflows at 1 m far from the cough source, such as velocity profile and turbulence. These studies built our basic understanding of the flow dynamics of an unobstructed cough jet and its effect on respiratory pathogen dispersion.

However, these studies mainly characterized the unobstructed cough jet or cough droplets in a large space. The cough jet and its development may be altered due to some unique physical settings in the environment. For example, in public transport cabins, gaspers are commonly installed above the passengers to provide proper thermal comfort. The overhead gasper jet can interact with and bent downward the cough jet. In addition, the backrest in front probably blocks the cough jet and changes the trajectory of a cough jet. Limited studies have focused on the cough jet interaction with the gasper jet and backrest in a cabin environment. Cao et al. [28,29] experimentally studied the airborne cough jet trajectory due to a downward plane jet by

86 smoke experiment and evaluated airborne infection risk of the front person in a chamber.
87 However, the flow field of the cough jet and the interaction process with the plane jet was not
88 analyzed and investigated. Li et al. [30] studied the trajectory of a gasper jet under the effect of
89 slit background flow in an aircraft cabin. They focused on the gasper jet trajectory, instead of
90 the cough jet trajectory. Yan et al. [31] and Lin et al. [32] studied the effect of cough jet on the
91 droplet dispersion and local airflow in an aircraft cabin by numerical simulation. But the gasper
92 jet was not involved in their studies. Recently, our group studied the cough droplet deposition
93 on nearby surfaces and airborne exposure of nearby passengers in a cabin environment under
94 the effect of the gasper jet and backrest [33]. These studies focused on the droplet distribution
95 or the airborne infection risk of nearby passengers. The cough jet was not visualized and
96 characterized, and the flow dynamics due to the gasper jet or backrest were not investigated in
97 detail. Since the flow dynamics of a cough jet and its interaction with gasper jet are essential
98 for the analysis of the aerosol dispersion and infection risk. Thus, further study of the cough
99 jet dynamics due to gasper jet and backrest is needed to understand cough droplet deposition
100 or dispersion in a cabin environment.

101 In this work, the objectives are to experimentally visualize the cough jet development, to study
102 the effect of gasper jet on the flow dynamics of the cough jet, and to suggest infection control
103 measures for public transportation. A four-seat setup was employed to simulate a cabin
104 environment. An artificial cough jet containing poly-dispersed droplets was released by a
105 verified cough generator to simulate the human cough. A PIV setup was used to characterize
106 the velocity field of the cough jet. The cough jet dynamics will directly determine the cough
107 droplet deposition on the front backrest. To correlate the cough jet dynamics and droplet
108 deposition, the distribution of cough droplets on the front backrest was measured by a
109 microscope.

2. Materials and methodology

2.1. Experimental setup and studied cases

A two-row four-seat setup and an air duct system were employed. The experimental setup has been used in our previous work [33]. Four identical thermal manikins were located at the four seats as shown in Fig. 1a. The manikin at the rear-left seat was considered as an infected passenger (IP). The front one was considered as the healthy passenger (HP). The heat generation of each thermal manikin was 75 W to simulate a sitting person with moderate activity [34]. The distance between the IP's mouth and HP's backrest was 0.5 m. The vertical distance between the jet outlet and the mouth was 0.3 m as shown in Fig. 1a and 1b. The diameter of the gasper outlet was 0.05 m. The gasper jet velocity at the same height of the mouth was measured and studied. The temperature and relative humidity of the room were controlled at 21±1 °C and 70%±3%, respectively. The background airflow velocity was measured to be less than 0.1 m/s.

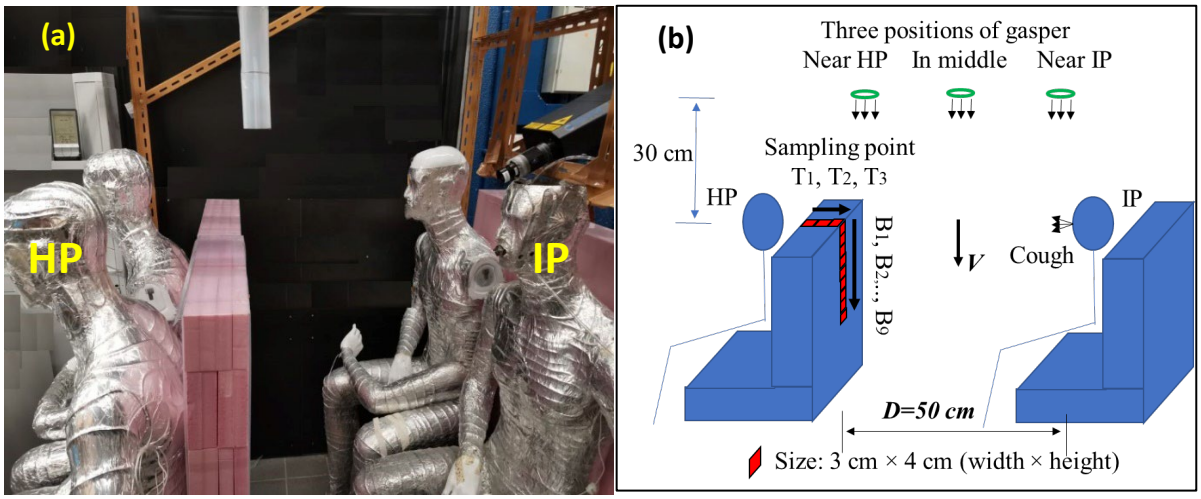

Figure 1 (a) Experimental setup and (b) schematic diagram of the experimental setup

A cough generator was used to simulate a real cough, which has been used in our previous work [35]. The releasing velocity of cough droplets was around 12 - 14 m/s and the peak droplet size was between 10 - 20 μm, which was similar to a real cough [5]. In the experiment, the IP

128 'coughed' 3 times with a time interval of 5 seconds, and each cough lasted 1 second. In each
129 cough, the generator released 0.075 mL artificial saliva solution. The artificial saliva solution
130 consisted of 12 g sodium chloride and 76 g glycerol in 1 L sterilized water [35,36]. Non-volatile
131 material in the solution accounted for around 6% in volume, similar to real human respiratory
132 fluid [37]. In this work, three positions of IP's gasper were studied including "Near HP", "In
133 middle", and "Near IP" as shown in Fig. 1b. Four gasper jet velocities were studied at 0 m/s,
134 0.75 m/s, 1.5 m/s, and 2.5 m/s.

135 2.2. Flow field measurement by PIV and deposited droplet measurement by microscope

136 Particle image velocimetry (PIV, LaVision Ltd) was employed to measure the velocity field of
137 the artificial cough jet. The cough droplets worked as the seeding particles. Thus, the trajectory
138 of cough droplets was directly measured. The laser generator was put above the head of IP or
139 HP to let the laser sheet cover the measurement areas, as shown in Fig. 1a. The CCD camera
140 was perpendicular to the laser sheet and the distance was adjustable to focus on the target areas.
141 The frequency of the double-exposure laser and camera was 5 Hz. The measurement lasted 20
142 s to capture the whole time series of the three coughs of the IP. The transient velocities were
143 calculated by the software and the mean velocity field can be calculated for each cough. The
144 detailed PIV parameters and image analysis by the software are described in previous papers
145 [35,38-40]. The size of each measurement area was 5 cm×7 cm. Multi areas were measured and
146 stitched together as shown in Fig. 2 in the section of results.

147 Polyvinyl Chloride (PVC) plates were attached to the backrest before the experiment for
148 droplet sampling. Three plates were on the top surface (noted as T_1, T_2, T_3) and nine plates
149 were on the back surface (noted as B_1, B_2, …, B_9) as shown in Fig. 1b. The size of each PVC
150 plate was 3 cm × 4 cm (width × height). After the deposition experiment and sample collection,
151 the droplets on the surface were then measured by a microscope (Ni-E, Nikon, Japan). The

detailed measurement method by the microscope can be seen in previous work [35]. Each experiment was triplicated.

3. Results

3.1. Cough jet development when gasper was "In middle" position

Fig. 2 shows the cough jet development and interaction with the backrest under the gasper velocity of 0 m/s. The mean velocity was calculated from transient flow fields. The cough jet was released from the IP's mouth and then traveled forward. When the cough jet met the backrest, the upper part continued traveling forward and should directly impinge on the front passenger's head. The lower part of the cough jet turned downward and traveled along the back surface of the backrest forming wall attached jet. At the corner of the backrest, a small portion of cough jet flowed upward and formed a small detour flow. The cough jet has a cone shape with an apex-angle of around 24^{o} as shown by the dashed line. It is almost identical with the opening angle of 23.9 ± 3.4^{o} of real human cough cloud [25]. The apex-angle is also similar to a free jet in a static environment [41]. If we set half of the maximal velocity as a critical value and plot the solid lines, the area covered by the solid lines can be noted as half velocity area. The width of the half velocity area roughly matched with the half-width of the cough jet, and the apex angle of the half velocity area (i.e. covered by solid lines) was around 12^{o}. The half velocity area can be regarded as the core part of the cough jet with high velocity and high concentration of droplets. As the increase of gasper jet velocity from 0 m/s to 2.5 m/s, the cough jet was no longer symmetrical to the centerline, but was bent downward gradually at the area beneath the gasper, as shown in Figure S1 in Supplementary Information.

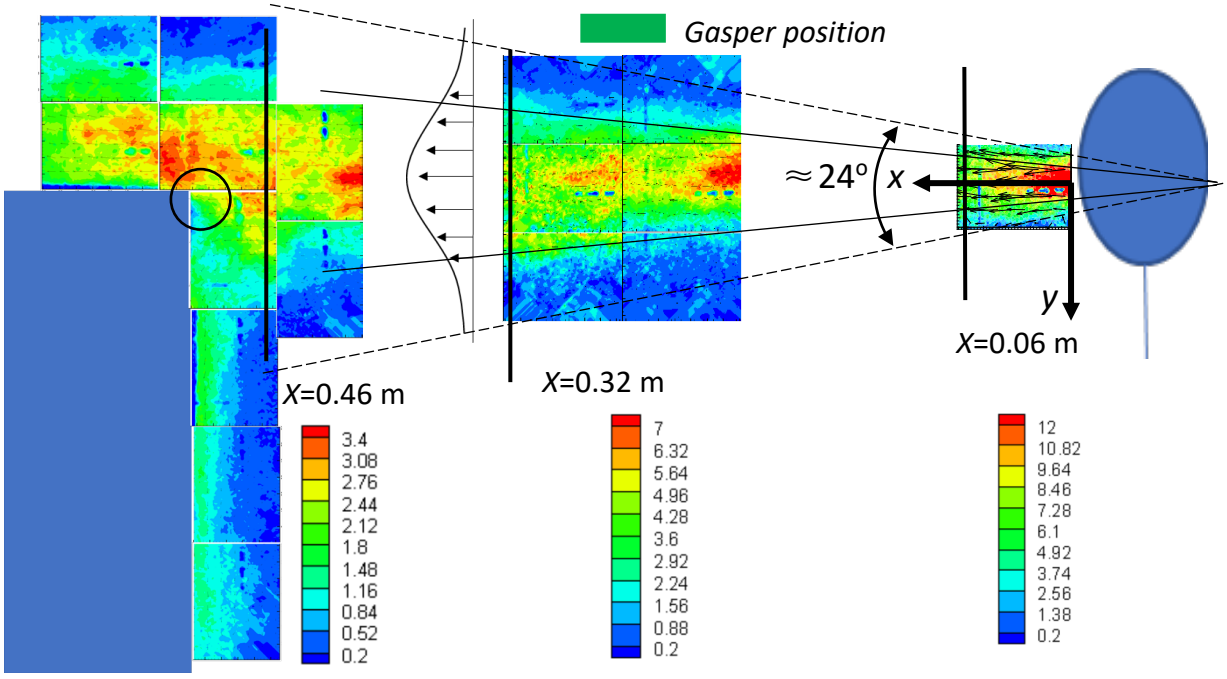

Figure 2. Cough jet development and interaction with backrest under gasper "In middle" with a velocity of 0 m/s. The unit of the velocity in the legend is m/s.

Fig. 3 shows the cough jet interaction with the backrest when the gasper was "In middle" with different velocities. The cough jet first impinged on the backrest and then was split into two portions. When the gasper jet velocity was 0 m/s or 0.75 m/s, the upper part of the cough jet continuously traveled forward in the horizontal direction. When the gasper jet velocity was 1.5 m/s, most of the cough jet impinged on the backrest and turned downward. A portion of the cough jet traveled upward/forward with an angle of around 45° and reattached to the top surface of the backrest. When the gasper jet velocity was 2.5 m/s, the whole cough jet impinged on the backrest at a much lower position and then most of the cough jet turned down along the back surface of the backrest. Only a small portion of the cough jet went upward after impingement. It indicates that the impingement area and cough jet width are important in determining where cough jet goes. As the increase of the gasper velocity from 0, to 0.75, to 1.5 and 2.5 m/s, the impingement region of the cough jet on the backrest was moved downward from around y = [0-0], to [0-1], to [1-5], and to [3-12] cm, as listed in Table 1.

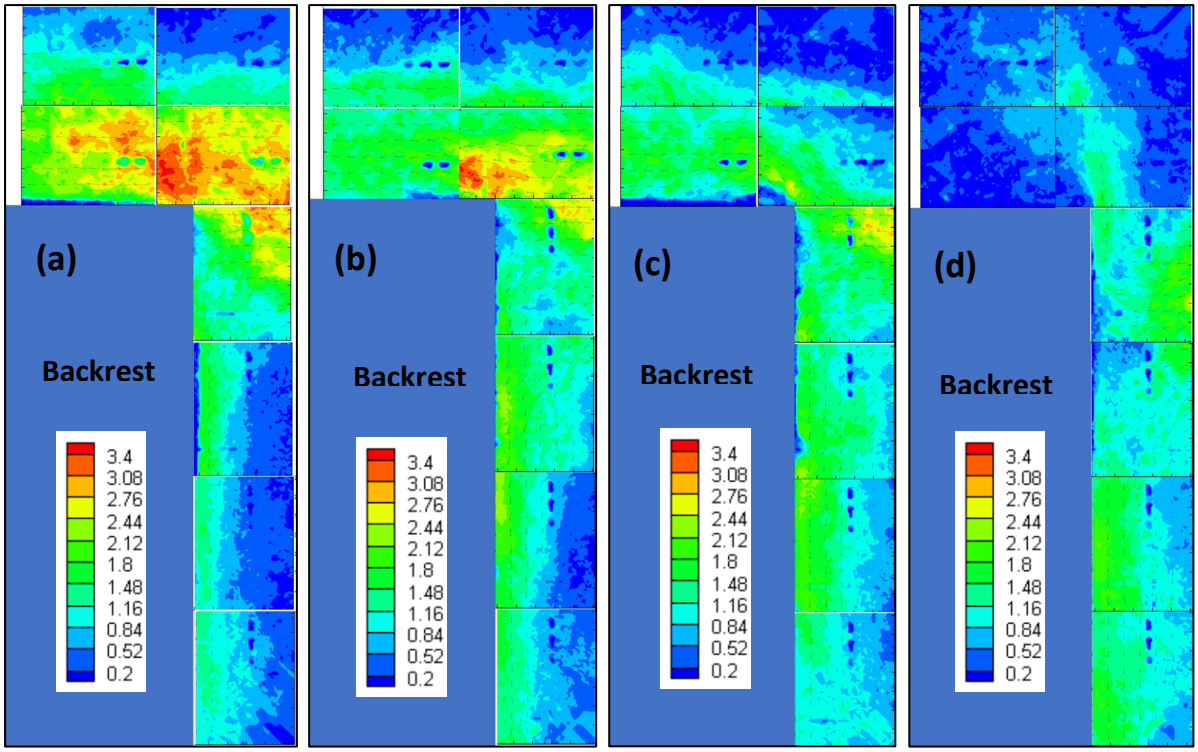

Figure 3. Cough jet interaction with backrest when the gasper was "In middle" with velocities of 0 m/s, 0.75 m/s, 1.5 m/s, and 2.5 m/s (a, b, c, and d)

3.2. Cough jet development when gasper was "Near IP" and "Near HP"

When the gasper was "Near IP", the cough jet was bent near IP's mouth. Then, the cough jet impinged on the backrest and split into two portions as shown in Figure S2 in Supplementary Information. The impingement point was lower than that when the gasper was "In middle". When the gasper was "Near HP", the cough jet was bent downward and then immediately impinged on the backrest as shown in Figure S3 in Supplementary Information. As the increase of the gasper jet velocity, the impingement region was lower on the backrest. As the gasper was closer to the IP, the impingement region was also lower on the backrest. The impingement region for each studied case by PIV was shown in Table 1.

3.3. Velocity profiles of cough jet at different x positions under the effect of gasper jet

When the gasper was “In middle”, velocity profile in the *x-direction* of the cough jet along the line of x = 0.32 m (i.e. just out of the main area of gasper jet, as shown in Fig. 2) was plotted in Fig. 4a. Thus, the velocity profile here can reflect the bending effect of the gasper jet. For the gasper jet velocity of 0 m/s, the velocity profile in the *x-direction* was almost symmetric to y = 0. As the increase of gasper jet velocity, the velocity profile was skewed upward, indicating that the cough droplets with high velocity were pushed down to a lower position. For the velocity of 2.5 m/s, the peak velocity was at y = 2.5 cm, and the upper part of the velocity profile was around 0 m/s. When the gasper was “Near IP”, the *x-direction* velocity profile of cough jet along the line of x = 0.06 m (i.e. immediately out of the main area of the gasper jet, as shown in Fig. 2) was plotted in Fig. 4b. The velocity profile here can represent the extent to which the gasper jet bends the cough jet. It was seen that the *x-direction* velocity profile was skewed upward gradually with the increase of gasper jet velocity. The peak value of the velocity profile was around 9 m/s. For the gasper jet with different velocities, peak values of the velocity profiles were similar. It indicated that the downward gasper jet did not directly affect the horizontal velocity of the cough jet in the interaction area but just bend the cough jet downward to some extent.

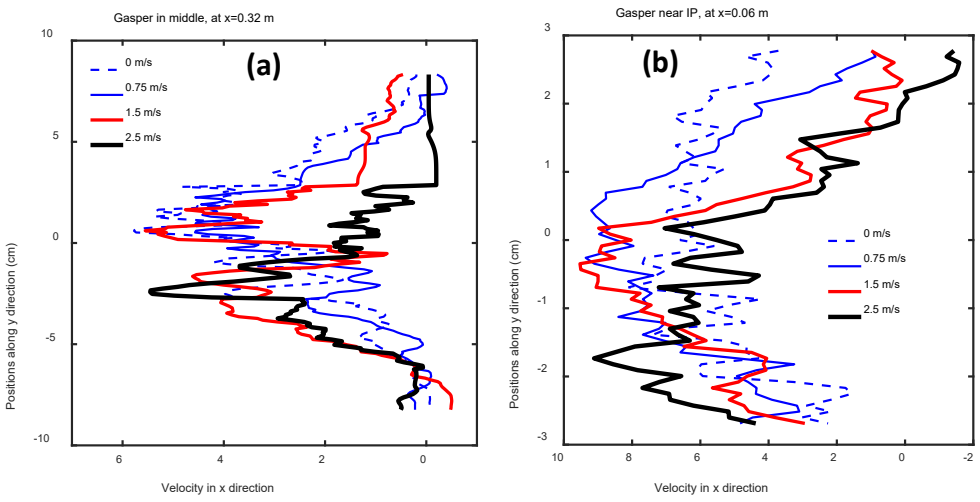

Figure 4. Velocity profile in x direction of cough jet along the (a) x = 0.32 m with gasper in middle and (b) x = 0.06 m with gasper near IP. The cough jet velocity near the interaction area for Fig. 4a (i.e. 4-6 m/s) is lower than that in Fig. 4b (i.e. 8-10 m/s).

The *x-direction* velocity profiles of cough jet along the line of x = 0.46 m (i.e. immediately before impingement, as shown in Fig. 2) with gasper at different positions were shown in Figure S4 in Supplementary Information. When the gasper was "Near HP", the velocity profile of cough jet was only slightly pushed downward with different gasper jet velocities. When the gasper was "In middle" or "Near IP", the velocity profile was skewed upward. When the gasper jet velocity was 2.5 m/s, the peak velocity appeared at y = 4 cm and 10 cm for the gasper position of "In middle" and "Near IP", respectively. It is also found that the peak value of the velocity profile was decreased with the increase of gasper jet velocity. For example, the peak values for the gasper jet of 0 m/s and 2.5 m/s were around 3.2 m/s and 2 m/s respectively for the gasper position of "Near IP".

The velocity profiles of cough jet in the *y-direction* with gasper at different positions were shown in Figure S5 in Supplementary Information. For the lower part of the cough jet, the velocity in the *y-direction* was positive indicating the downward direction. The gasper jet can enhance the downward velocity and the enhancement was increased with the increase of gasper jet velocity.

3.4. Cough droplet distribution on the backrest

Fig. 5 shows the cough droplet distribution on the top and back surfaces of the backrest with the gasper in middle. The back surface (e.g. point B_1, B_2, …, B_9) of the backrest was directly facing the coming cough jet, and the top surface (e.g. point T_1, T_2, T_3) was parallel to the cough jet direction. For the gasper jet with different velocities, the highest droplet concentration happens on the back surface of point B_1. The droplet concentration decreased gradually from

point B_1 to B_9 along the back surface. For the gasper jet velocity of 0 m/s - 1.5 m/s, the highest droplet concentration at point B_1 was around 1.7×10^4 #/cm^2, containing droplets larger than 50 μm, while for the velocity of 2.5 m/s, the droplet concentration was around 1.1×10^4 #/cm^2 and the droplets were mainly smaller than 50 μm. It is expected that the gasper jet with a higher velocity can blow away more droplets from the cough jet, and then reduce the possibility of droplet accumulation on the impingement region. Thus, a higher velocity of the gasper jet can lead to a smaller size of droplets deposited on the backrest. For the top surface of the backrest, the droplet concentrations at gasper velocity of 0 m/s and 0.75 m/s were higher than that at gasper velocity of 1.5 m/s and 2.5 m/s. It was because there were less cough droplets traveled above the top surface with the increase of gasper jet velocity, as indicated in Fig. 3. For the gasper jet velocity of 0 m/s and 0.75 m/s, the droplet concentration of point T_3 was lower than that at point T_2. It was because that the cough jet formed a small counterclockwise vortex above the point T_3 as shown in Fig. 3. Overall, the gasper jet with a higher velocity can cause the lower deposition on both top surface and back surface of the backrest.

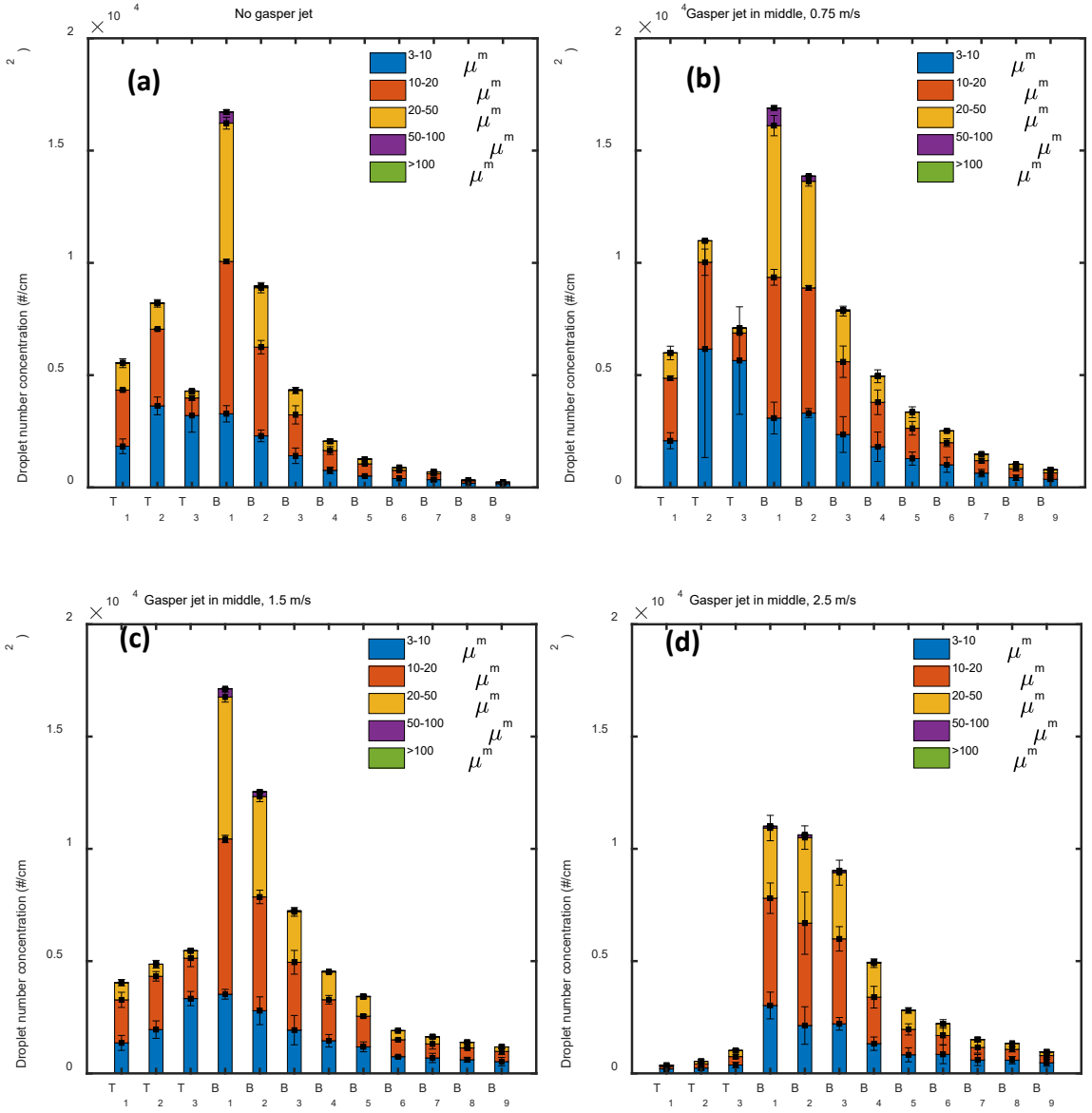

Figure 5. Cough droplet distribution on top and back surfaces of backrest when gasper jet velocity is 0 m/s, 0.75 m/s, 1.5 m/s, and 2.5 m/s (a, b, c, and d).

When the gasper was “Near IP” or “Near HP”, the droplet distribution on the top and back surface of the backrest was similar to that when the gasper was “In middle”, as shown in Figure S6 and Figure S7 in Supplementary Information. The droplet concentration on the back surface was lowest when the gasper was “Near IP” with a velocity of 2.5 m/s. The high concentration areas of the deposited droplets for each case were summarized and listed in Table 1. It is found that the high droplet concentration areas matched well with the direct impingement regions by

PIV measurement. It indicates that the gasper jet firstly affects the flow dynamics of the cough jet and then changes droplet deposition on the front backrest.

4. Model development and analysis of the cough jet trajectory

In this work, the gasper jet and cough jet velocity changes along the *x* direction. In our modeling, we discretize the horizontal distance *x* into *n* sections and the length of each section *i* is *dx*, as shown in Fig. 6a. The parameters of gasper jet and cough jet in each section *i* are assumed to be the constants. The value of each parameter will change along the *x-direction*. To be concise, the parameter value in section *i* is written as the form of $P(i)$ in the following modeling, such as $x(i)$ and $V(i)$.

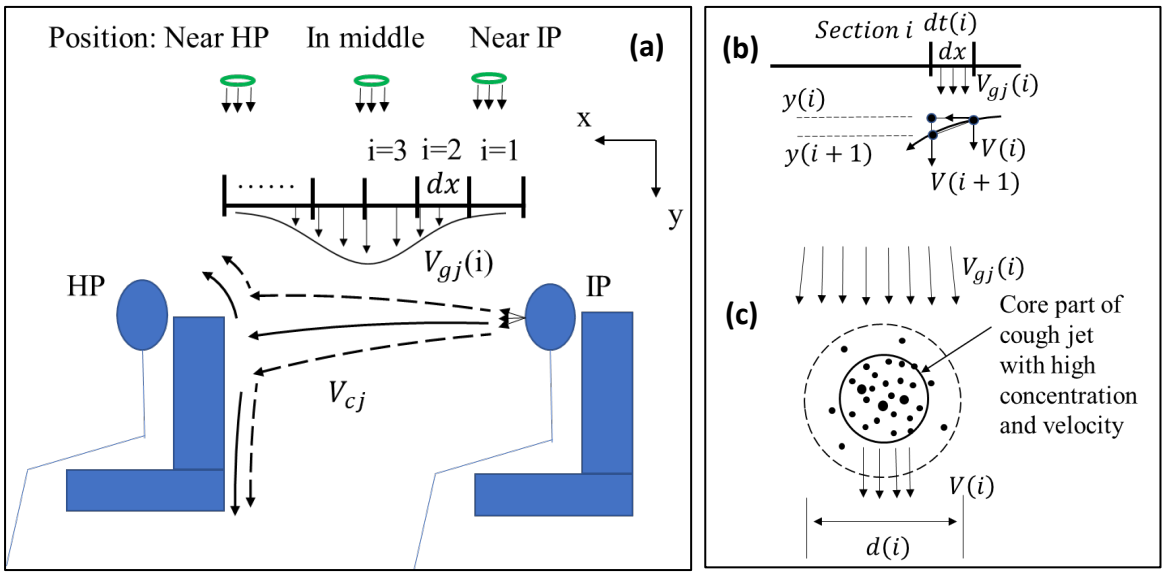

Figure 6 Schematic diagram of (a) cough jet and gasper jet, (b) cough jet trajectory in section *i*, and (c) impingement of gasper jet on cough jet

4.1. Parameters of the cough jet and gasper jet

The cough jet was pushed downward by the gasper jet and collided with the front backrest. The trajectory of cough jet before impingement was affected by the gasper position and gasper jet velocity. The origin of the coordinate was set at the mouth of the IP. The gasper velocity along

285 *x* direction was not uniform. The schematic diagram of the gasper jet velocity is shown in Fig.
286 6a. The gaper jet velocity profile $V_{gj}(i)$ along *x-direction* can be described by a Gaussian
287 equation [42]:

288 $$V_{gj}(i) = V_{gj\_max} \cdot \exp[-((x(i) - x_0)/h)^2] \quad (1)$$

289 $$x(i) = dx \cdot i \quad (1a)$$

290 where V_{gj_max} is the centerline velocity of gasper jet along *x* direction at *y* = 0, $x(i)$ is the *x*
291 position of section *i*, x_0 is the *x* position of gasper jet centerline, which is equal to 0.025, 0.25,
292 and 0.475 m for "Near IP", "In middle", and "Near HP" respectively, h is a constant with value
293 of 0.05, dx is the length of each section. Equation (1) describes the gasper jet velocity profile
294 along *x-direction* for three different gasper positions. The details are shown in Figure S8 in
295 Supplementary Information.

296 The centerline velocity of the cough jet will decay gradually as it moved forward, as indicated
297 in Fig. 2. The velocity of a cough jet, $V_{cj}(i)$, can be described by Equation (2) for a fully
298 developed turbulent jet [28].

299 $$V_{cj}(i) = V_{c0} \cdot k \cdot (x(i)/d_0)^{-1} \quad (2)$$

300 where V_{c0} is the initial velocity of cough jet with value of 13.5 m/s, k is a constant with value
301 of 2.4 for fully developed region [28], $d_0$is initial diameter of the cough jet with value of 0.04
302 m. The details are shown in Figure S9 in Supplementary Information.

303 4.2. Model development for the trajectory of cough jet

304 During each section *i*, the gasper jet with downward velocity of $V_{gj}(i)$ will impinge on the
305 cough jet with downward velocity of $V(i)$ as shown in Fig. 6b and c. It is assumed that after
306 the impingement both the gasper jet velocity and cough jet velocity reached the same value of

$V_{gasper}(i)$ due to the gasper jet. Based on the momentum conservation, Equation (3) for $V_{gasper}(i+1)$ during each section *i* can be deduced:

$$V_{gasper}(i+1) = \frac{V_{gj}(i)\cdot m_{gj}(i)+V(i)\cdot m_{cj}(i)}{(m_{cj}(i)+m_{gj}(i))} \quad (3)$$

$$m_{gj}(i) = \rho_{gj}\cdot\left(V_{gj}(i)-V(i)\right)\cdot dt(i)\cdot d(i)\cdot dx \quad (3a)$$

$$m_{cj}(i) = \rho_{cj}(i)\cdot\pi\left(\frac{d(i)}{2}\right)^2\cdot dx \quad (3b)$$

$$dt(i) = \frac{dx}{V_{cj}(i)} \quad (3c)$$

where $m_{gj}(i)$ is the mass of the gasper jet impinging on the cough jet in section *i*, $m_{cj}(i)$ is the mass of the cough jet in section *i*, ρ_{gj} is density of gasper jet, $\rho_{cj}(i)$ is density of cough jet consisting of saliva and cough air, $V_{gj}(i)$ is velocity of gasper jet in section i, $d(i)$ is the cough jet diameter at section *i*, $V(i)$ is the downward cough jet velocity at the beginning of section *i*, $dt(i)$ is the time of cough jet passing section *i*. The details of each parameter are shown in Figure S10 in Supplementary Information. In addition, during the section *i*, the cough jet was also subjected to the buoyancy force and gravitational force due to the density difference. Thus, the cough jet velocity change of $dV_{density}(i)$ due to density difference can be calculated by the force analysis and kinematic method as Equation (4):

$$dV_{density}(i) = g\cdot\left(1-\frac{\rho_{air}}{\rho_{cj}(i)}\right)\cdot dt(i) \quad (4)$$

where g is the gravitational acceleration, ρ_{air} is density of surrounding air. The details are shown in Figure S11 in Supplementary Information. Thus, the downward velocity of the cough jet at the end of section *i* as shown in Fig. 6b can be expressed as Equation (5):

$$V(i+1) = V_{gasper}(i+1) + dV_{density}(i) \quad (5)$$

In addition, for section i as shown in Fig. 6b, the cough jet trajectory was changed from $y(i)$ to $y(i+1)$ due to the gasper jet and buoyancy force. The value of $y(i+1)$ consists of $y(i)$ and movement of $V(i) \cdot dt(i)$. The cough jet trajectory, $y(i+1)$, can be calculated by Equation (6).

$$y(i+1) = y(i) + V(i) \cdot dt(i) \quad (6)$$

where the initial value $y(0)$ is set as 0, the initial value $V(0)$ is set as 0, the initial value of $dt(0)$ is set as 0. Then, the downward velocity of cough jet and the trajectory of cough jet can be calculated.

4.3. Predicted trajectory of cough jet with different gasper position and velocity

The trajectory of the cough jet was modeled, and the predicted trajectories of the cough jet centerline are shown in Fig. 7. When the gasper was "Near IP", the cough jet was bent at the beginning near the IP's mouth, especially for the velocity of 2.5 m/s. Then, the cough jet impinged on the backrest at the lower position of the backrest. While, for the gasper "In middle", the cough jet was bent at the middle of the area. For the gasper "Near HP", the cough jet was bent near the backrest and then impinged on the backrest at a higher position than other gasper positions. The predicted trajectories and impingement points matched well with the experimental results by PIV measurement, as shown in Table 1. The boundary of the cough jet can then be obtained based on the centerline trajectory of the cough jet and the apex angle of the cone shape of the cough jet.

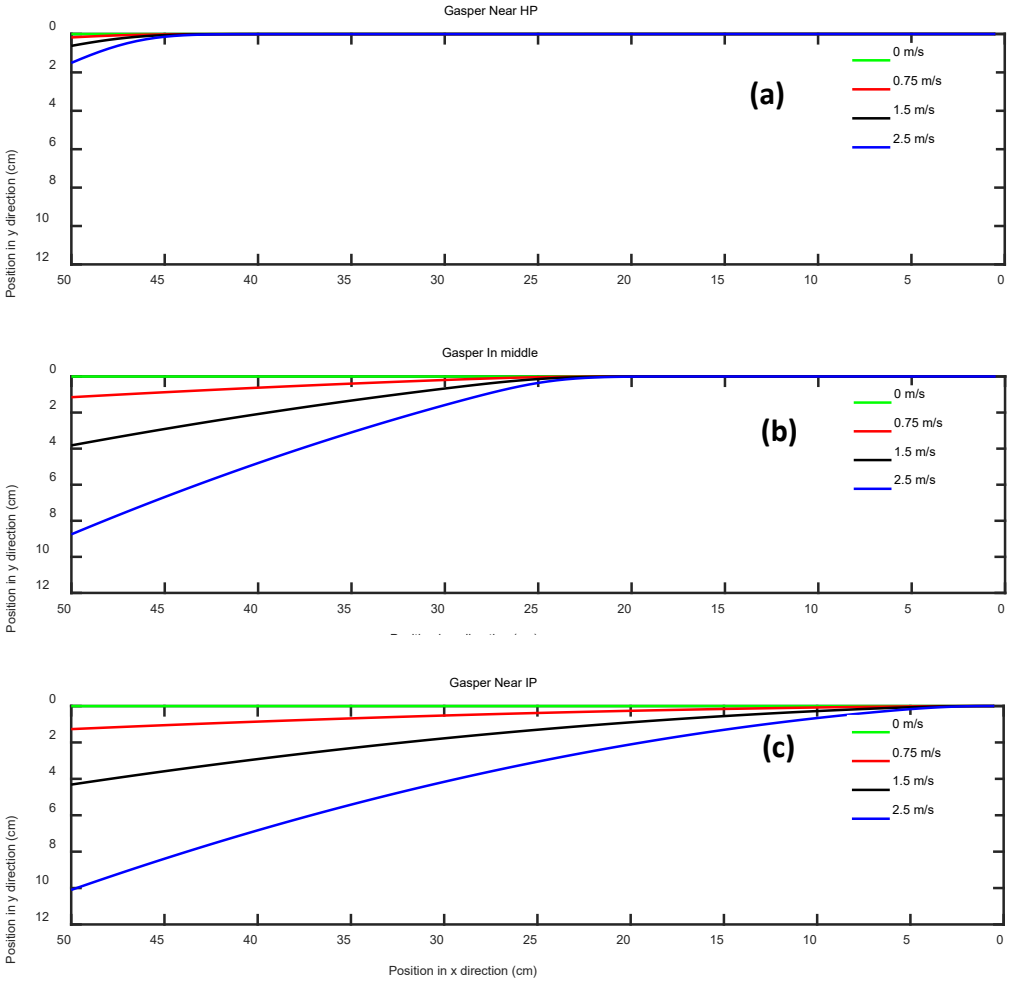

Figure 7. Predicted cough jet trajectory with gasper at the position of (a) "Near HP", i.e. x = 47.5 cm, (b) "In middle", i.e. x = 25 cm, and (c) "Near IP", i.e. x = 2.5 cm.

Table 1. Direct impingement region from PIV, peak concentration region of deposited droplets, and predicted impingement point in the y axis

Position	**Near IP**			**In middle**			**Near HP**		
(y-axis)	PIV	Droplet	Predicted	PIV	Droplet	Predicted	PIV	Droplet	Predicted
0 m/s	0	[0-4]	0	0	[0-4]	0	0	[0-4]	0
0.75 m/s	[0-3]	[0-4]	1.3	[0-1]	[0-4]	1.2	[0-1]	[0-4]	0.2
1.5 m/s	[0-7]	[0-8]	4.3	[1-5]	[0-8]	3.8	[0-2]	[0-4]	0.6
2.5 m/s	[6-12]	[8-12]	10.1	[3-12]	[0-12]	8.8	[0-4]	[0-4]	1.5

"PIV" means the direct impingement region measured by the PIV experiment; "Droplet" means the peak concentration region of deposited droplets in Section 3.4; "Predicted" means the impingement point calculated by the developed model in Section 4.

The downward velocity of the cough jet when traveling forward was also plotted based on the developed model and was shown in Figure S12 in Supplementary Information. The cough jet started to acquire downward velocity almost linearly when entering the area of the gasper jet. For example, the start point was around *x* of 40 cm, 20 cm, and 0 cm for the gasper position of "Near HP", "In middle", and "Near IP", respectively. The cough jet velocity in the *y-direction* when reaching the backrest of the front seat was around 0.9 m/s, 1.0 m/s, and 0.8 m/s for these three gasper positions respectively. It matched well with the *y-direction* velocity measured by PIV shown in Figure S5 in Supplementary Information.

4.4. Effect of cough jet temperature, inside droplet, and velocity profile on cough jet trajectory

In this work, the cough jet is an isothermal jet with the same temperature as the surrounding air. The real cough jet is a humid and warm jet with a temperature of around 37 ^{o}C, for which the cough air density is around 1.111 kg/m^3. To study the effect of cough jet temperature, the trajectories of a warm cough jet and an isothermal cough jet were calculated and compared based on the developed model, as shown in Figure S13. It indicated that the warm cough jet has almost the same trajectory as the isothermal cough jet at the short-range. The effect of cough droplets in the cough jet was also studied. The cough jet without droplets also had almost the same trajectory as the normal cough jet. To evaluate the effect of gasper jet velocity profile, a uniform crossflow with a velocity of 2.5 m/s was employed and compared with a normal gasper jet with a Gaussian velocity profile. We can see that at the position *x* of 50 cm, the *y* position value of the cough jet under the uniform crossflow was around 241% of the cough jet under the effect of a normal gasper jet. It indicated that for the cough jet at the short range, the velocity profile of the gasper jet has a dominant effect on cough jet trajectory compared with the buoyancy force or inside droplets.

5 Discussion

Previously researchers mainly focused on the unobstructed cough jet and characterized its velocity field [18,19,24]. It is the first study to analyze the flow dynamics of the obstructed cough jet in a cabin environment, which is affected by the backrest and gasper jet. Some implications were proposed based on the new findings in this work.

5.1. Backrest and gasper jet could be compensation for not keeping social distance in public transportation

For an unobstructed cough jet, large droplets separate from the cough jet and deposit onto the ground at the distance of 1.5 m – 2 m [6]. Small aerosols are still contained in the cough jet and travel forward. Thus, WHO or CDC has a social distance of around 1 m - 2 m to prevent droplet spray [10,11]. Many researchers suggest enlarging the social distance to prevent direct exposure to aerosol jets. While, in public transportation such as airplanes and buses, the distance between each row is less than 1 m, indicating the difficulty to maintain social distance. In this work, it is found that when gasper jet with a velocity of 2.5 m/s, the cough jet impinged on a rather lower position of the backrest and then almost totally turned downward. Thus, the front passenger avoids both the droplet spray and direct exposure to high concentration airborne aerosols, which has a similar effect of keeping social distance. Thus, the backrest and gasper jet could be compensation for not keeping social distance in public transportation.

5.2. Further mitigation of airborne exposure may rely on localized exhaust

The backrest and gasper jet redirect cough jet downward but do not remove respiratory aerosols out of the public transport cabin. Background ventilation can dilute and remove respiratory aerosols from the environment [43,44]. But the mixing effect of background ventilation disperses aerosols to the whole cabin environment before removing the aerosols from the cabin.

For this scenario, the localized exhausts under each seat are suggested to timely exhaust the high concentration aerosols at the ground level before the dispersion to the whole environment.

5.3. Surface cleaning of the backrest should be conducted to mitigate fomite route

It is found that when the cough jet was bent by the gasper jet of 2.5 m/s, the deposition on top surface (i.e. frequently touched area) of the backrest was also greatly reduced. It indicated that the gasper jet can mitigate the fomite route to some extent, which agrees with our previous work [33]. But the back surface of the backrest contains a large number of droplets, although the number is reduced with the increase of gasper jet velocity. Thus, the back surface of the backrest should be frequently cleaned, which contains more large respiratory droplets, to mitigate the fomite route. In addition, the droplet distribution on the backrest can be the boundary condition for the infection risk analysis for the fomite route.

5.4. Cough jet trajectory model is applicable for the jet with an arbitrary velocity profile

The interaction of one jet with another is common in the industry or building environments. Previously, the effective velocity ratio of two jets was employed to calculate the jet trajectory in a uniform crossflow [45,46]. It cannot be directly used for the crossflow with a velocity profile. To employ the crossflow theory, some researchers normalized the coordinates [30] or modify the constants [28] to calculate the jet trajectory. The modified constants are limited to the specific experimental setup and are not universal. Differently, the proposed model in this work for jet trajectory employs momentum conservation and discretization of the airflow. It can be employed to calculate the jet trajectory under the effect of another jet with an arbitrary velocity profile. Thus, the proposed model is universal for different scenarios. For example, the personalized ventilation (PV) airflow can protect the user by blocking the cough jet, in which the PV flow interacts with the cough jet. In the aircraft cabin, the slit airflow of background ventilation interacts with and redirects the gasper jet.

It is also found by modeling that the inside droplets and buoyancy almost do not affect the cough jet trajectory in the short-range. It indicates that the simplified iso-thermal coughing or sneezing jet by smoke or CO_2 is acceptable for the study of short-range cough jet behavior. The calculation of droplets in modeling short-range cough jet trajectory can be simplified. While for the study of long-range cough jet trajectory, this simplification is not suitable because large droplets will separate from cough jet [6].

5.5. Limitations

The gasper jets in different public transportation have different initial diameters and blowing angles. In this work, we only considered the gasper jet blowing downward with one diameter. In addition, the background ventilation in the chamber was not the same as that in an aircraft cabin or bus. The background airflow pattern also varied with different public transport cabins. More work is needed to study cough jet development under different ventilation types. The relative humidity during the experiment was around 70%. It represents some of the practical situations, such as the buses in tropical or sub-tropical areas. For the environment with a lower relative humidity such as an aircraft cabin, the cough jet dynamics may be a little bit different from the results in this work. The gasper jet for all studied cases in this work is blowing downward to simplify the study of different positions of the gasper jet. In practice, the gasper is usually directed to the breathing zone of the passenger and may be at a slightly oblique angle. The exhaled air is usually warmer than the surrounding air and may cause the jet bend upward, while the cough jet in this work has the same temperature as the surrounding environment. The interaction of gasper jet with cough jet in *z-direction* is not studied in this work. The gasper jet impinges first on the cough jet and then flows around the cylindrical cough jet. As the velocity of gasper jet varies, the flow field of gasper jet after impingement should also change in *z-direction*. This work mainly investigated the bulk flow of the cough jet under the effect of the

gasper jet by PIV technique. The turbulence from the cough jet and its effect on particle concentration were not involved in this study. But the turbulence by the cough jet/gasper jet could contribute to the dispersion of cough droplets and affect the infection risk of nearby passengers. Thus, future work is needed to systematically study the turbulence introduced by the cough jet/gasper jet and reveal its effect on droplet dispersion.

6. Conclusion

In this work, the flow dynamics of a cough jet in a cabin environment was studied by the PIV technique. It was found that cough jet traveled forward and then impinged on the backrest. After the impingement, upper part of the cough jet would continue traveling forward and spray on the front passenger. When the gasper jet with velocity of around 2.5 m/s, the cough jet was bent downward and redirected to the ground level by the backrest. Thus, the front passenger can avoid the droplet spray and direct exposure to airborne aerosols. It indicated that the backrest and gasper jet can be compensation for not keeping social distance in public transportation. The localized exhaust beneath each seat was suggested to timely remove the bulk aerosols at the ground level. A model was proposed to predict the cough jet trajectory, which was applicable for the jet with arbitrary velocity profile. The results in this work could enhance our understanding of cough jet development and help develop infection control measures in public transportation.

Acknowledgement

The work was supported by the Collaborative Research Fund (CRF) project (no. C1105-20G) and the General Research Fund (no. 17207121) granted by the Research Grants Council of the Hong Kong Special Administrative Region, China.

Declarations of competing interest

The authors declare that they have no known competing financial interests or personal relationships that could have appeared to influence the work reported in this paper.

References

[1] Dye C, Gay N. Modeling the SARS epidemic. Science 2003;300:1884-5.

[2] Liu Y, Ning Z, Chen Y, Guo M, Liu Y, Gali NK et al. Aerodynamic analysis of SARS-CoV-2 in two Wuhan hospitals. Nature 2020;582:557-60.

[3] De Wit E, Van Doremalen N, Falzarano D, Munster VJ. SARS and MERS: recent insights into emerging coronaviruses. Nat Rev Microbiol 2016;14:523.

[4] Gupta JK, Lin C, Chen Q. Transport of expiratory droplets in an aircraft cabin. Indoor Air 2011;21:3-11.

[5] Chao CYH, Wan MP, Morawska L, Johnson GR, Ristovski ZD, Hargreaves M et al. Characterization of expiration air jets and droplet size distributions immediately at the mouth opening. J Aerosol Sci 2009;40:122-33.

[6] Xie X, Li Y, Chwang A, Ho PL, Seto WH. How far droplets can move in indoor environments–revisiting the Wells evaporation–falling curve. Indoor Air 2007;17:211-25.

[7] Liu L, Wei J, Li Y, Ooi A. Evaporation and dispersion of respiratory droplets from coughing. Indoor Air 2017;27:179-90.

[8] Wells WF. Airborne Contagion and Air Hygiene. An Ecological Study of Droplet Infections. Airborne Contagion and Air Hygiene. An Ecological Study of Droplet Infections. 1955.

493 [9] Wells WF. ON AIR-borne infection: study II. Droplets and droplet nuclei. Am J Epidemiol
494 1934;20:611-8.

495 [10] CDC. Coronavirus Disease 2019 (COVID-19): What is social distancing? 2020.

496 [11] WHO. Coronavirus disease (COVID-19) advice for the public. 2020.

497 [12] Bahl P, Doolan C, de Silva C, Chughtai AA, Bourouiba L, MacIntyre CR. Airborne or
498 droplet precautions for health workers treating COVID-19? J Infect Dis 2020.

499 [13] Bourouiba L. Turbulent gas clouds and respiratory pathogen emissions: potential
500 implications for reducing transmission of COVID-19. JAMA 2020;323:1837-8.

501 [14] Morawska L, Cao J. Airborne transmission of SARS-CoV-2: The world should face the
502 reality. Environ Int 2020;139:105730.

503 [15] Prather KA, Marr LC, Schooley RT, McDiarmid MA, Wilson ME, Milton DK. Airborne
504 transmission of SARS-CoV-2. Science 2020;370:303-4.

505 [16] Morawska L, Milton DK. It is time to address airborne transmission of coronavirus disease
506 2019 (COVID-19). Clin Infect Dis 2020;71:2311-3.

507 [17] Jimenez J, Marr L, Randall K, Ewing ET, Bourouiba L. Echoes Through Time: The
508 Historical Origins of the Droplet Dogma and its Role in the Misidentification of Airborne
509 Respiratory Infection Transmission. Available at SSRN 2021.

510 [18] VanSciver M, Miller S, Hertzberg J. Particle image velocimetry of human cough. Aerosol
511 Sci Technol 2011;45:415-22.

512 [19] Gupta JK, Lin C, Chen Q. Flow dynamics and characterization of a cough. Indoor Air
513 2009;19:517-25.

514 [20] Dudalski N, Mohamed A, Mubareka S, Bi R, Zhang C, Savory E. Experimental
515 investigation of far-field human cough airflows from healthy and influenza-infected subjects.
516 Indoor Air 2020;30:966-77.

517 [21] Tang JW, Liebner TJ, Craven BA, Settles GS. A schlieren optical study of the human
518 cough with and without wearing masks for aerosol infection control. J R Soc Interface
519 2009;6:S727-36.

520 [22] Li H, Leong FY, Xu G, Ge Z, Kang CW, Lim KH. Dispersion of evaporating cough
521 droplets in tropical outdoor environment. Phys Fluids 2020;32:113301.

522 [23] Wei J, Li Y. Enhanced spread of expiratory droplets by turbulence in a cough jet. Build
523 Environ 2015;93:86-96.

524 [24] Redrow J, Mao S, Celik I, Posada JA, Feng Z. Modeling the evaporation and dispersion
525 of airborne sputum droplets expelled from a human cough. Build Environ 2011;46:2042-51.

526 [25] Bourouiba L, Dehandschoewercker E, Bush JW. Violent expiratory events: on coughing
527 and sneezing. J Fluid Mech 2014;745:537-63.

528 [26] Ge H, Chen L, Xu C, Cui X. Large-eddy simulation of droplet-laden cough jets with a
529 realistic manikin model. Indoor Built Environ 2021:1420326X211032247.

530 [27] Liu S, Novoselac A. Transport of airborne particles from an unobstructed cough jet.
531 Aerosol Sci Technol 2014;48:1183-94.

[28] Cao G, Liu S, Boor BE, Novoselac A. Dynamic interaction of a downward plane jet and a cough jet with respect to particle transmission: An analytical and experimental study. J Occup Environ Hyg 2017;14:618-31.

[29] Cao G, Liu S, Boor BE, Novoselac A. Characterizing the dynamic interactions and exposure implications of a particle-laden cough jet with different room airflow regimes produced by low and high momentum jets. Aerosol Air Qual Res 2015;15:1955-66.

[30] Li J, Liu J, Dai S, Guo Y, Jiang N, Yang W. PIV experimental research on gasper jets interacting with the main ventilation in an aircraft cabin. Build Environ 2018;138:149-59.

[31] Yan Y, Li X, Yang L, Yan P, Tu J. Evaluation of cough-jet effects on the transport characteristics of respiratory-induced contaminants in airline passengers' local environments. Build Environ 2020;183:107206.

[32] Yang L, Li X, Yan Y, Tu J. Effects of cough-jet on airflow and contaminant transport in an airliner cabin section. J Comput Multiph Flows 2018;10:72-82.

[33] Wang C, Xu J, Fu SC, Chan KC, Chao CY. Respiratory bioaerosol deposition from a cough and recovery of viable viruses on nearby seats in a cabin environment. Indoor Air 2021;31:1913-25.

[34] ASHRAE. ASHRAE Handbook-Fundamentals. 2021.

[35] Wang CT, Fu SC, Chao CY. Short-range bioaerosol deposition and recovery of viable viruses and bacteria on surfaces from a cough and implications for respiratory disease transmission. Aerosol Sci Technol 2020;55:215-30.

552 [36] Wang CT, Leung WT, Xu JC, Fu SC, Chao CY. Droplet detachment behavior from a
553 rough hydrophilic surface. J Aerosol Sci 2020;139:105469.

554 [37] Effros RM, Hoagland KW, Bosbous M, Castillo D, Foss B, Dunning M et al. Dilution of
555 respiratory solutes in exhaled condensates. Am J Respir Crit Care Med 2002;165:663-9.

556 [38] Wang C, Xu Y, Wu Y, An Z. PIV investigation of the flow features of double and single
557 45° up-pumping pitched blade turbines in a square tank. Can J Chem Eng 2018;96:788-99.

558 [39] Xu Y, Wang C, Wu Y. Optimization of mechanical accelerated clarifier based on
559 numerical simulation of flow field. Adv Mech Eng 2017;9:1687814017720881.

560 [40] Xu J, Fu S, Chao CY. Performance of airflow distance from personalized ventilation on
561 personal exposure to airborne droplets from different orientations. Indoor Built Environ
562 2020:1420326X20951245.

563 [41] Or CM, Lam KM, Liu P. Potential core lengths of round jets in stagnant and moving
564 environments. J Hydro-environ Res 2011;5:81-91.

565 [42] Xia LP, Lam KM. Velocity and concentration measurements in initial region of submerged
566 round jets in stagnant environment and in coflow. J Hydro-environ Res 2009;3:21-34.

567 [43] Tang JW, Li Y, Eames I, Chan P, Ridgway GL. Factors involved in the aerosol
568 transmission of infection and control of ventilation in healthcare premises. J Hosp Infect
569 2006;64:100-14.

570 [44] Li Y, Leung GM, Tang JW, Yang X, Chao CY, Lin JZ et al. Role of ventilation in airborne
571 transmission of infectious agents in the built environment-a multidisciplinary systematic
572 review. Indoor Air 2007;17:2-18.

573 [45] Broadwell JE, Breidenthal RE. Structure and mixing of a transverse jet in incompressible
574 flow. J Fluid Mech 1984;148:405-12.

575 [46] Muppidi S, Mahesh K. Study of trajectories of jets in crossflow using direct numerical
576 simulations. J Fluid Mech 2005;530:81.